Investigating Bacterial Motion Near Walls in Low Reynolds Number Non-Newtonian Fluids

Qitao Duan

Hunan University, Changsha 410000, China

duanqitao@hnu.edu.cn

Abstract. Bacterial motion in non-Newtonian fluids is influenced by ciliary propulsion modes (push/pull), fluid rheological properties, and wall effects, with the interaction of these factors resulting in diverse movement behaviors. However, the quantitative mechanisms by which these factors affect the average velocity of bacteria remain unclear. This study utilizes the COMSOL Multiphysics simulation platform to develop a rigid two-dimensional ellipsoidal bacterial model and conducts numerical simulations within a square micro-scale Carreau fluid domain. By introducing magnetic force constraints to inhibit near-wall adhesion, the study systematically explores the coupling effects of these factors. The results indicate that: (1) the ciliary propulsion mode primarily determines the average velocity, and fluid properties (relaxation time λ, power index n) significantly influence this velocity response; (2) wall constraint effects are pronounced, with the average velocity of bacteria in the x-direction reduced by approximately 86% at a distance of 50 μm from the wall compared to the far-field value. This research provides a theoretical foundation for the active regulation of microbial motion in complex fluid environments.

Keywords: Bacteria; Self-propulsion; Wall effects; Magnetic constraints; Carreau fluid; Surface shear rate; Numerical simulation.

1. Introduction

The mechanisms of microbial motion in complex fluid environments are a leading topic in the field of microscale biomechanics. Bacteria, as a type of microorganism, are closely linked to human health; for instance, during infections, large quantities of bacteria can be present in the blood, a quintessential example of a shear-thinning non-Newtonian fluid. In recent years, there has been rapid progress in bacteria-driven targeted drug delivery systems[1] and bio-inspired micro-nano robotics[2]. A key challenge is to gain a deeper understanding of bacterial dynamics in complex non-Newtonian fluids, such as blood. Research has shown that bacterial taxis is significantly enhanced in shear-thinning fluids[3]; the presence of power-law fluids in porous media can destabilize thermal-biological convection, affecting bacterial spatial distribution[4]; and increased bacterial concentration can hinder fluid flow, necessitating optimization through buoyancy parameter adjustments[5]. Thus, studying the motion characteristics of bacteria in non-Newtonian fluids is not only of fundamental scientific significance but also essential for advancing related biomedical applications.

Current research has made substantial strides in understanding microbial dynamics. Early work by Theers et al. (2016)[6] introduced an analytically solvable model for ellipsoidal swimmers, revealing through mesoscopic particle dynamics (MPC) simulations that two puller-type swimmers can form a stable wedge-shaped cooperative configuration via fluid interactions in confined environments, with stability depending on wall constraints and the anisotropy of the swimmers. Theers et al. (2018)[7] subsequently uncovered the antagonistic effects of fluid dynamics on phase separation in micro-swimmers: suppressing phase separation in spherical systems while enhancing aggregation in ellipsoidal systems. In 2020, Qi et al.[8] demonstrated through mesoscopic simulations the competitive mechanisms of shape and active stress in the rheological behaviors of spherical pullers, ellipsoidal swimmers, and ciliates. That same year, Tsang et al.[9] introduced reinforcement learning into the design of low Reynolds number swimming strategies, proposing a novel paradigm for self-learning micro-swimmers. In 2021, Meng et al.[10] quantitatively linked the dynamics of single-flagellated bacteria to the asynchronous wave characteristics at the array scale, bridging a theoretical gap from "individual behavior to collective dynamics". In 2022, Steinkühler et al.[11] revealed the fluid dynamic

behaviors of substrate gradient-driven bacterial micro-compartments (MCP) in acellular systems for the first time. More recently, Hosaka et al. (2023)[12] uncovered the chiral dynamics of linear micro-swimmers in non-Newtonian fluids through theoretical modeling and numerical simulations, highlighting how such fluids can drive transitions in directional movement patterns and oscillatory behaviors in push-pull swimmer pairs[13]. The latest research by Hosaka et al. (2024)[14] found that non-Newtonian fluids can induce unique chiral tendencies in micro-swimmers: pushers align in a bimodal fashion along the non-Newtonian axis, while pullers are constrained to move within a vertical plane. In the same year, Piro et al.[15] revealed the critical influence of the geometric shape of micro-swimmers on their navigation energy consumption.

However, despite significant advancements, current research primarily focuses on the autonomous movement patterns of microorganisms in Newtonian fluids[4]. Non-Newtonian fluids, which are prevalent in both natural and engineering contexts, exhibit viscoelastic effects that can substantially alter the swimming characteristics of bacteria[16]. For instance, colloidal suspensions can enhance bacterial swimming efficiency by up to 80% by suppressing flagellar oscillations. Factors such as shear-thinning (or thickening) effects, normal stress differences, and microstructural evolution in non-Newtonian fluids often lead to complex nonlinear dynamic responses in microbial motion. In weak shear-thinning fluids, the curvature of bacterial circular trajectories decreases, whereas in viscoelastic fluids, curvature changes are governed by the propulsion mode of the microorganisms (e.g. decreased curvature for pushers and increased curvature for pullers)[2]. Additionally, pulsating flows within porous media can significantly reduce flow velocity due to the presence of microorganisms, necessitating the optimization of buoyancy and biological convection parameters[17]. Crucially, existing theoretical models still lack the predictive capability to adequately characterize the strong coupling between “fluid-microbe” interactions at the microscale, making it challenging to unify the effects of shear and viscoelasticity (e.g. the bacterial sliding motion model in Carreau-Yasuda mucus[18]). This limitation severely constrains the application potential of related technologies: in targeted precision medicine for gut microbiota, inaccuracies in predicting the penetration efficiency of carrier microorganisms in intestinal mucus (a typical shear-thinning fluid) can lead to failures in delivery system targeting[19][1]. In the context of pollutant biodegradation, the absence of a convective instability model for power-law fluids and microorganisms in porous soil environments hinders the optimization and efficiency of degrading bacterial distributions[20].

To address these theoretical and practical challenges, this study employs the COMSOL Multiphysics simulation platform to develop a numerical model of bacterial motion in Carreau-type non-Newtonian fluids. It systematically explores the fluid-structure interaction (FSI) mechanisms under varying fluid parameters that characterize shear-thinning properties and viscoelasticity. By integrating computational fluid dynamics (CFD) with micro-mechanical analysis, this research aims to elucidate how key factors, such as the viscoelastic effects of fluids and their memory characteristics, regulate microbial propulsion speed. The findings will provide theoretical guidance for optimizing the environmental adaptability of microorganism-driven systems, facilitating the transition of biomimetic micro-robot designs from theoretical modeling and ideal experimental conditions to real-world complex applications.

2. Fundamental Modeling

2.1 Model Simplification

The research represents the bacteria as an ellipsoid, as shown in Figure 1**a**, which has a capsule-like shape. The Reynolds number Re is defined as:

$$\mathrm{Re} = \frac{\text{Inertial Force}}{\text{Viscous Force}} = \frac{\rho' v l}{\mu} \tag{1}$$

In this equation, ρ' represents the fluid density, v is the characteristic flow velocity, l is the characteristic length, and μ is the dynamic viscosity of the fluid. Low Reynolds number is generally defined as $\mathrm{Re} \ll 1$. Due to the small characteristic length (size) l of bacteria, their motion in the

fluid is classified as low Reynolds number motion. According to Equation (1), the viscous force dominates the motion of bacteria in low Reynolds number fluids, while their own inertial forces can be neglected. The elastic deformation of the bacterial body has a minimal impact on the disturbance of the flow field[21], and the period of bacterial motion is greater than the relaxation time of its deformation. Therefore, in the subsequent studies, we will treat bacteria as rigid materials with a density of ρ.

To study the near-wall motion of bacteria near the wall of an infinite fluid domain, we first define the bacterial dimensions with a semi-major axis $\mathrm{a} = 5\mu\mathrm{m}$ and a semi-minor axis $\mathrm{b} = 3\mu\mathrm{m}$, $\mathrm{c} = \sqrt{\mathrm{a}^2 - \mathrm{b}^2}$. Next, we define the fluid domain as a square with dimension of $2500\mu\mathrm{m}$, which is significantly larger than the size of the bacteria. Then the equations of motion for the bacteria are formulated. To avoid boundary effects on bacterial motion, we position the bacteria at the exact center of the fluid domain and derive the equations while in a stationary state.

The motion of bacteria in the fluid generates oscillations. To simulate the approximate linear motion of bacteria in the fluid, the study applies a pair of equal and opposite forces at two points on the bacteria, creating a rotational couple. The bacterial model and the applied couple are illustrated in **Figure 1 a**. This rotational couple satisfies:

$$\boldsymbol{F} \cdot \boldsymbol{L} = 0 \tag{2}$$

$$\boldsymbol{F} \times \boldsymbol{L} = \boldsymbol{k_1} \tag{3}$$

Here, $\boldsymbol{L}$ is the vector between the two points of application, $\boldsymbol{F}$ is the net force at the points of application, and $\boldsymbol{k_1}$ is a parameter whose direction is perpendicular to the plane formed by $\boldsymbol{F}$ and $\boldsymbol{L}$, allowing control over the self-regulation speed of the bacteria. Equation (2) indicates that the component of the force at the points of application is always perpendicular to the long axis of the ellipse, while Equation (3) provides the relationship between the magnitudes of $\boldsymbol{F}$ and $\boldsymbol{L}$.

According to Theers et al.[7], to derive the velocity formula at the surface of the ellipse in a Cartesian coordinate system, the research presents the transformation relationship between elliptical and Cartesian coordinates:

$$\xi = \frac{x}{\mathrm{a}}, \tau = \frac{\mathrm{a}}{\mathrm{c}} \tag{4}$$

Thus, we can derive formulas using elliptical coordinates based on the elliptical eccentric angle and Cartesian coordinates. Considering that the bacteria's cilia and flagella have self-propelling capabilities[22], the study applies a wall shear velocity to the surface of the bacteria, represented by the following equation:

$$\boldsymbol{u_{sq}} = -B_1\left(\boldsymbol{e_\xi} \cdot \boldsymbol{e_x}\right)(1 + \beta\xi)\boldsymbol{e_\xi} \tag{5}$$

Here, B_1 is related to the self-propelling speed of the bacteria, given by:

$$U_0 = B_1(\tau(\tau - (\tau^2 - 1)\mathrm{coth}^{-1}(\tau))) \tag{6}$$

In Equation (5), $\boldsymbol{e_\xi}$ is the unit tangent vector at the surface of the ellipse, with the counterclockwise direction considered positive; $\boldsymbol{e_x}$ is the unit vector in the positive x-direction; and β is a state parameter, where $\beta > 0$ represents pulling motion and $\beta < 0$ represents pushing motion. [8][14] defines the elliptical parameter coordinates as:

$$x = \mathrm{a}\cos\theta \qquad y = \mathrm{b}\sin\theta \tag{7}$$

Here, the eccentric angle of the ellipse is included in the definition of the parameter coordinates. Combining with the tangent vector:

$$\boldsymbol{\xi}' = \left(\frac{\mathrm{d}x}{\mathrm{d}\theta}, \frac{\mathrm{d}y}{\mathrm{d}\theta}\right) = (-\mathrm{a}\sin\theta, \mathrm{b}\cos\theta) \tag{8}$$

After normalization, we can obtain:

$$\boldsymbol{e_\xi} = \left(\frac{-\mathrm{a}\sin\theta}{\sqrt{(\mathrm{a}\sin\theta)^2 + (\mathrm{b}\cos\theta)^2}}, \frac{\mathrm{b}\cos\theta}{\sqrt{(\mathrm{a}\sin\theta)^2 + (\mathrm{b}\cos\theta)^2}}\right) \tag{9}$$

For the unit vector along the x-axis $\boldsymbol{e_x}$, this research computes the product:

$$\boldsymbol{e_\xi} \cdot \boldsymbol{e_x} = \frac{-\mathrm{a}\sin\theta}{\sqrt{(\mathrm{a}\sin\theta)^2 + (\mathrm{b}\cos\theta)^2}} \tag{10}$$

Substituting into Equation (5) can determine the magnitude of u_{sq}:

$$u_{sq} = B_1(1 + \frac{\beta x}{\mathrm{a}})(\frac{\mathrm{asin}\theta}{\sqrt{(\mathrm{asin}\theta)^2+(\mathrm{bcos}\theta)^2}}) \quad (11)$$

2.2 Establishment of Body-Fixed Coordinates

In the context of variable computations in COMSOL, x is defined as the coordinate of any point on the bacteria in space. Since the equation established in Section 2.1 (Equation 11) is applicable only to the bacteria, directly using this derived formula would introduce significant errors during bacterial motion. Therefore, this study needs to establish a coordinate system fixed to the bacteria that aligns with the application range of Equation (11). Considering that the bacteria undergo both translation and rotation during their movement, the study defines the relationship between the body-fixed coordinates X, Y and the spatial coordinates x, y as follows:

$$x = x_c + X\cos\alpha - Y\sin\alpha \quad (12)$$

$$y = y_c + X\sin\alpha + Y\cos\alpha \quad (13)$$

Here, x_c and y_c represent the coordinates of the centroid of the ellipse, and α is the angle of rotation of the ellipse.

we define the spatial coordinates of two points in **Figure 1 a**, A and B, on the ellipse at any given time as follows:

$$\mathrm{A}(x_1, y_1) \quad , \quad \mathrm{B}(x_2, y_2)$$

At the initial moment, the spatial coordinates of points A and B are:

$$\mathrm{A}_0\left(-\frac{\mathrm{a}}{2}, 0\right) \quad , \quad \mathrm{B}_0(\frac{\mathrm{a}}{2}, 0)$$

These coordinates are known, and by substituting them, we can solve for x_c and y_c:

$$X = x\cos\alpha + y\sin\alpha - x_c\cos\alpha \ - y_c\sin\alpha \quad (14)$$

$$Y = x_c\sin\alpha \ - y_c\cos\alpha - x\sin\alpha + y\cos\alpha \quad (15)$$

Here:

$$\cos\alpha = \frac{x_2-x_1}{\mathrm{a}} \quad , \quad \sin\alpha = \frac{y_2-y_1}{\mathrm{a}} \quad (16)$$

To meet the computational requirements, x and y in Equations (7) and (11) can be replaced with X and Y, respectively. Thus, Equations (7) and (11) can be modified to:

$$X = a\cos\theta \qquad Y = b\sin\theta \quad (17)$$

$$u_{sq} = B_1(1 + \frac{\beta X}{\mathrm{a}})(\frac{\mathrm{asin}\theta}{\sqrt{(\mathrm{asin}\theta)^2+(\mathrm{bcos}\theta)^2}}) \quad (18)$$

By importing Equations (2), (3), and (18) into COMSOL and substituting $\beta = 3$, the study can conduct a simulation, resulting in the bacterial motion time series shown in **Figure 1 b**. The figure indicates that the bacteria do not exhibit rotational motion, approximating linear motion. The body-fixed coordinates are used solely for accurate calculations; when referring to directions in the following text, this study will still adhere to the direction of the spatial coordinates.

2.3 Equation Verification

To verify whether Equation (18) in COMSOL aligns with theoretical results, this study employs Python to establish a coordinate system where the arc length serves as the horizontal axis and the surface shear velocity u_{sq} as the vertical axis. The right vertex is designated as the origin, with counterclockwise rotation indicating the positive direction of the arc length. The research generates plots of surface shear velocity as a function of arc length for three cases: positive, negative, and zero β. The arc length is calculated using the second kind of elliptical integral:

$$\mathrm{E}(\varphi, k) = \int_0^{\varphi} \sqrt{1 - k^2\sin^2\theta}\,\mathrm{d}\theta \quad (19)$$

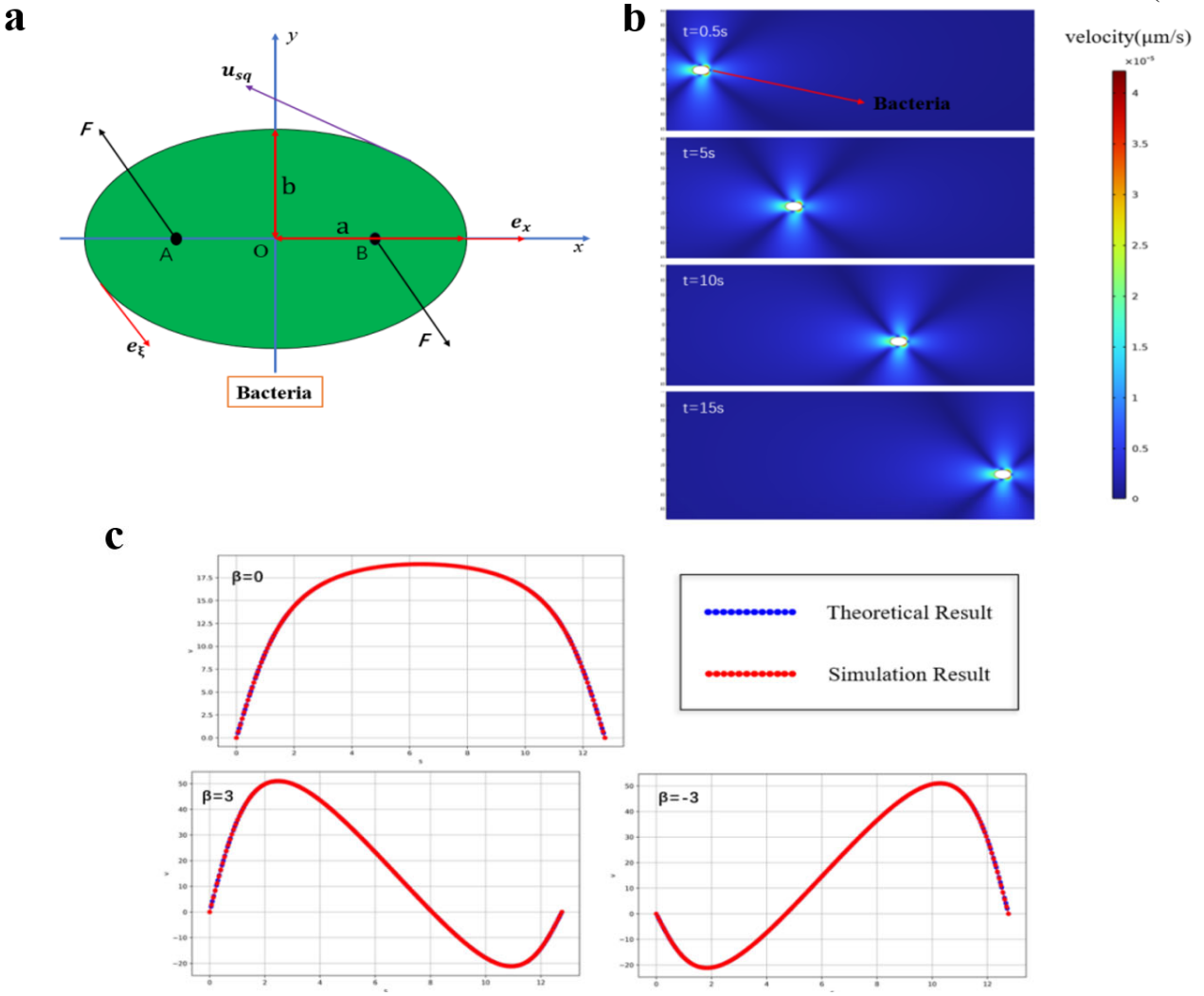

Figure 1 a illustrates a schematic of the bacteria. The long axis measures $2a = 10\mu m$, and the short axis measures $2b = 6\mu m$, with an applied torque. $\boldsymbol{u_{sq}}$represents the surface shear velocity. Figure 1 b shows the motion of the bacteria at $0.5s, 5s, 10s, 15s$ seconds, where different colors in the legend indicate varying fluid velocities. Figure 1 c depicts the variation of the surface shear velocity magnitude u_{sq} as a function of arc length s for $\beta = 0,3 - 3$. The results from Python and COMSOL are presented in the same plot, with blue representing theoretical results and red indicating simulation results.

The results are presented in **Figure 1 c**. The graphs generated in Python closely match those produced by COMSOL, demonstrating a strong consistency between the simulation results and theoretical predictions.

2.4 Fluid Properties

A significant challenge in bacteria-driven targeted drug delivery is understanding the kinetic response of microorganisms in non-Newtonian fluids. Based on this scientific motivation and aimed at applications in targeted drug delivery, we choose blood as a representative medium. Blood exhibits notable shear-thinning characteristics, making it well-suited for characterization using the Carreau model, which describes how viscosity changes with shear rate. Drawing on study[23], the study models the fluid domain using the Carreau model equation as follows:

$$\mu(\dot{\gamma}) = \mu_{inf} + (\mu_0 - \mu_{inf})[1 + (\lambda\dot{\gamma})^2]^{\frac{n-1}{2}} \quad (20)$$

The study can also specify the parameter values in Equation (20): $\mu_0 = 0.013\text{pa}\cdot\text{s}$, $\mu_{inf} = 0.003\text{pa}\cdot\text{s}$, $\lambda = 0.5\text{s}$, $n = 0.4$, $\rho = 1050\text{kg/m}^3$. Here μ_0 represents the zero-shear-rate viscosity, μ_{inf} denotes the viscosity at infinite shear rate, λ is the relaxation time, n is the power index, ρ refers to the bacterial density, and $\dot{\gamma}$ represents the shear strain rate.

Let L be the distance from the lower boundary of the fluid domain to the geometric center of the bacteria. According to Equation (20), the study will explore not only the magnitude of L and its effects but also how L is influenced by different modes of motion, represented by varying values of β, and different viscoelastic effects, indicated by varying relaxation times λ and power indices n. The relaxation time λ is the characteristic time at which viscosity begins to decrease significantly, reflecting the fluid's "memory effect". When $\lambda = 0$, the fluid behaves as a Newtonian fluid; when $\lambda > 0$, it behaves as a non-Newtonian fluid. Changes in the power index reflect the shear properties of the fluid: $n < 1$ indicates shear thinning, $n > 1$ indicates shear thickening, and $n = 1$ corresponds to a Newtonian fluid, which is equivalent to $\lambda = 0$.

3. Investigation Results

3.1 Introduction of Magnetic Force

we positioned the bacteria near the lower wall of the fluid domain to examine how the distance from the wall influences bacterial velocity. The average velocity at the center of the bacteria is defined as V. Using L as the horizontal coordinate and V as the vertical coordinate, we constructed a function graph of bacterial motion. Each point on the graph represents the arithmetic mean of instantaneous velocities calculated over 0.02-second intervals within a fixed 20-second period.

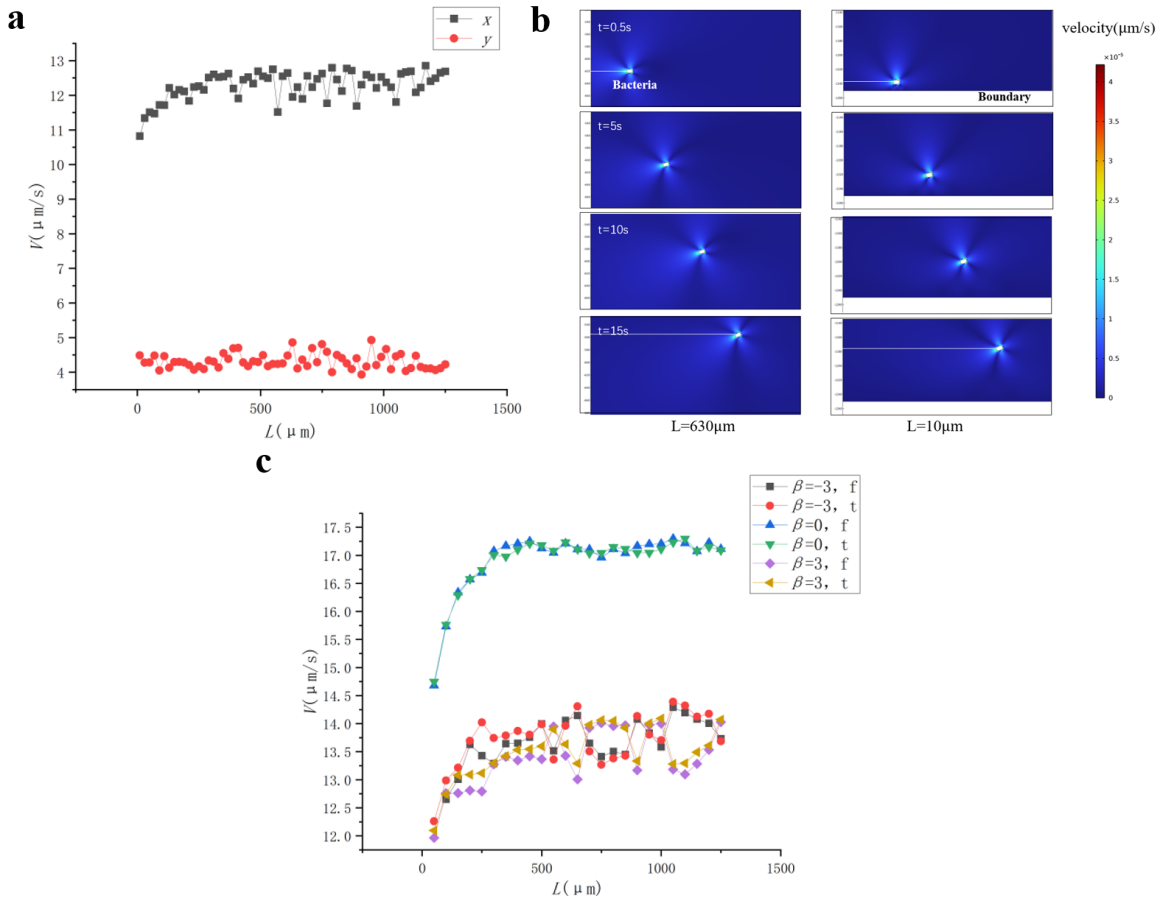

Figure 2 a illustrates the variations in x-direction and y-direction velocities at different values of L, with L intervals set at $20\mu\text{m}$. Figure 2 b depicts the time evolution of bacterial motion for $L = 630\mu\text{m}$ and $L = 10\mu\text{m}$. The side scale indicates spatial coordinates. In the $L = 630\mu\text{m}$ image, at

$t = 0.5\text{s}$, the bacteria are located at $L = 631\mu\text{m}$, and at $t = 15\text{s}$, they are at $L = 693\mu\text{m}$; these positions are marked with white lines. In the $L = 10\mu\text{m}$ image, at $t = 0.5\text{s}$, the bacteria are at $L = 13\mu\text{m}$, and at $t = 15\text{s}$, they are at $L = 74\mu\text{m}$, also indicated by white lines. Figure 2 c compares the x-direction velocities of bacteria with and without the application of magnetic force at $\lambda = 0.5\text{s}$ for various values of β, with L measured at $50\mu\text{m}$ intervals. In the legend, f denotes the absence of magnetic force, while t indicates its presence.

In COMSOL, the study inputs the five parameters mentioned earlier. Starting from $L = 10\mu\text{m}$, the study recorded the average velocities in the *x* and *y* directions at intervals of $20\mu\text{m}$ from the geometric center of the bacteria. The resulting graph is shown in **Figure 2 a**. The results indicate that as the bacteria move away from the wall, the velocity in the *x* direction gradually increases, while the velocity in the *y* direction decreases slightly.

The calculated time evolution of motion is illustrated in **Figure 2 b**. When close to the wall, the bacteria exhibit a strong tendency to swim toward the center of the fluid domain, resulting in a higher velocity in the *y* direction. Velocity measurements using point probes indicate that this *y*-direction movement causes a displacement that leads the bacteria to move away from the wall.

To investigate whether changes in *y*-direction velocity significantly affect *x*-direction velocity, the study introduced a magnetic force $\boldsymbol{F_b}$ to constrain y-direction displacement.

$$F_b = k_2\bar{y} \tag{21}$$

we define the magnitude of the magnetic force to be proportional to the displacement of the bacteria, with k_2 as the proportionality constant and $\bar{\boldsymbol{y}}$ representing the displacement in the *y* direction. The objective of introducing this force is to keep the *y*-direction displacement of the bacteria as close to zero as possible, allowing for horizontal linear motion in the *x* direction. Additionally, to prevent issues such as the rotation of the bacteria, we have conducted multiple calculations based on previous discussions and determined the parameter values for equations (3) and (21): $k_1 = 40\mu\text{N}\cdot\text{m}$, $k_2 = 0.5\text{N/m}$.

The study compared the simulation results with and without the introduction of magnetic force under the same parameter conditions, as illustrated in **Figure 2 c**. The calculations indicate that when $\beta = -3$ and L is very small (i.e. when the bacteria are close to the wall), the bacteria tend to move toward the wall and collide with it. While the introduction of the magnetic force does lead to a slight increase in velocity in the x direction, this increase is negligible for practical applications. Nonetheless, incorporating the magnetic force ensures that the bacteria do not collide with the wall when L is small, allowing for their continuous motion in the *x* direction within narrow conduit.

3.2 Effects of Different Parameters on Bacterial Velocity

3.2.1 Changes in Relaxation Time

By varying the relaxation time λ in the fluid properties according to equation (20), the study obtained three types of fluids characterized by different relaxation times: $\lambda = 0$, $\lambda = 0.5\text{s}$, and $\lambda = 1\text{s}$. Each case was illustrated with graphs that included varying values of β (specifically, $\beta = -3$, $\beta = 0$, and $\beta = 3$). In these graphs, the independent variable is the distance from the wall L, while the dependent variable is the average velocity V of the bacteria in the x direction.

The effects of changing relaxation time are depicted in **Figure 3 a, b, c**. It is evident from these graphs that, for different values of β, the average velocity of the bacteria is highest when $\lambda = 0$ compared to the cases of $\lambda = 0.5\text{s}$ and $\lambda = 1\text{s}$. Additionally, there is a clear trend showing that as λ increases, the average velocity decreases. When $\lambda \neq 0$, the maximum average velocity occurs at $\beta = 0$; conversely, when $\lambda = 0$, the maximum average velocity is observed for $\beta = 3$.

In exploring the impact of the wall on bacterial average velocity, all three graphs indicate that when $L \leq 250\mu\text{m}$, the average velocity of the bacteria increases with increasing distance from the wall. However, when $L \geq 250\mu\text{m}$, the average velocity stabilizes.

From the definition of β in equation (5), it is clear that $\beta < 0$ and $\beta > 0$ represent two opposing behaviors namely, pushing and pulling motions. The graphs also reveal a phenomenon where, at the same distance from the wall, the average velocities exhibit a "numerical inversion", indicating a sudden reversal in monotonicity within that range. This paired existence further corroborates the presence of two distinct modes of motion.

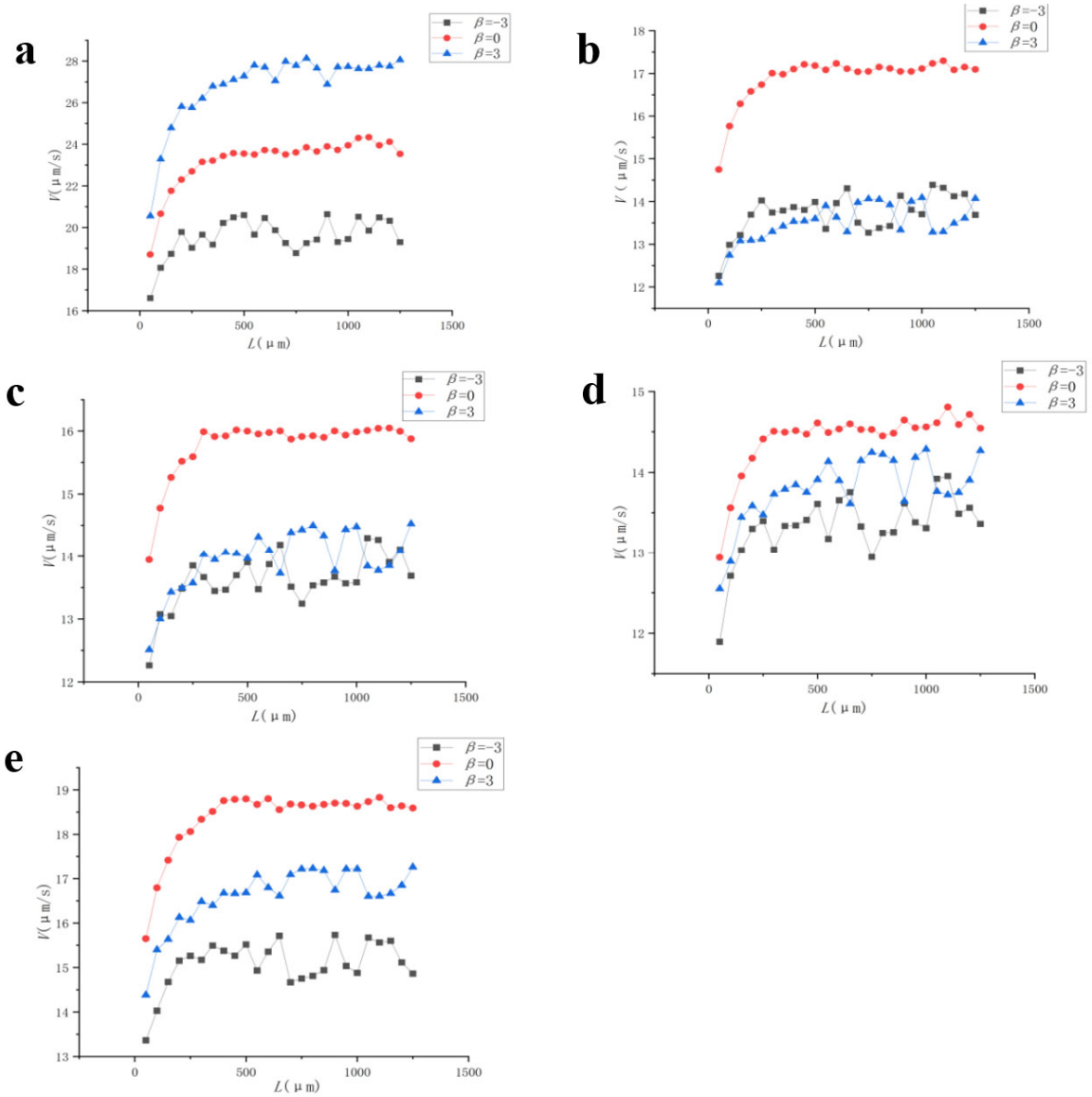

Figure 3 displays the variations in average velocity V of bacteria at different values of L for three distinct β values under varying λ and n. Panel a presents the data for $\lambda = 0$, $n = 0.4$ (or $\lambda = 1$, $n = 1$). Panel b corresponds to $\lambda = 0.5\text{s}$, $n = 0.4$. Panel c illustrates the scenario for $\lambda = 1\text{s}$, $n = 0.4$. Panel d shows the results for $\lambda = 1\text{s}$, $n = 0.1$, while panel e depicts the data for $\lambda = 1\text{s}$, $n = 0.7$.

3.2.2 Changes in Power Index

By fixing $\lambda = 1\text{s}$ and varying the power index n in the fluid properties according to equation (20), the study obtained three types of fluids characterized by different power indices: $n = 0.1, n = 0.4, n = 0.7$. These correspond to **Figure 3d**, **c**, and **e** respectively. Since the equation at $\lambda = 0$ is equivalent to that at $n = 1$, we will analyze the average velocities under different power indices using **Figure 3 d, c, e, a**.

The graphs indicate that as n increases, the average velocity of the bacteria rises for all values of β. From **Figure 3 e** and **a**, the study observes that when $n \geq 0.7$, the average velocity at $\beta = 3$

exceeds that at $\beta = -3$. Additionally, when $n = 1$, the maximum average velocity is achieved at $\beta = 3$, confirming previous findings.

By selecting data for different β values at $L = 50\mu m$ (initial movement distance) and $L = 500\mu m$ (data stabilization distance), the study conducted a ratio calculation and averaged the results. This analysis reveals that at $\boldsymbol{\beta} = -3(\text{pusher}), \beta = 0(\text{neutral}), \beta = 3(\text{puller})$, the wall restricts the average velocity of the bacteria in the x direction by approximately $86.00\%, 84.85\%, 86.06\%$.

4. Conclusion

This study establishes a numerical simulation framework using a rigid two-dimensional elliptical model of bacteria in Carreau-type non-Newtonian fluids, systematically revealing the dynamics of bacterial self-propulsion in low Reynolds number near-wall environments. The simulation results demonstrate that the mode of bacterial propulsion, whether push-like ($\beta < 0$) or pull-like ($\beta > 0$), exerts a decisive influence on average velocity, with significant differences and even reversals in velocity relationships observed under the same fluid parameters. This highlights the complexity of the interaction between propulsion modes and the flow field. The characteristics of non-Newtonian fluids, particularly the relaxation time λ representing viscoelastic memory effects, and the power index n reflecting shear-thinning behavior, play a crucial role in regulating bacterial motion. An increase in λ $(0 \rightarrow 1\text{s})$ generally suppresses propulsion efficiency, while an increase in n $(0.1 \rightarrow 0.7)$ significantly enhances velocity, particularly when $n \geq 0.7$, where the advantages of pull-like motion $(\beta = 3)$ become pronounced. The wall confinement effect is particularly significant, as the average velocity of bacteria in the x direction at a distance of $50\mu m$ from the wall is reduced by 84.85% to 86.06% compared to the far-field condition (at $L \geq 250\mu m$), confirming the strong inhibitory effect of the near-wall flow structure on microbial motion. Additionally, the introduction of magnetic constraints to address near-wall adhesion issues has been shown to effectively maintain horizontal trajectory stability, providing a viable control strategy for microchannel applications.

References

[1] Zhang, X., et al. Targeting to tumor-harbored bacteria for precision tumor therapy. ACS Nano, 2022.

[2] Zhao, Y., et al. Micro/nano-motors for enhanced tumor diagnosis and therapy. International Journal of Molecular Sciences, 2025, 26(16): 7684.

[3] Torres Maldonado, G., Kaya, T., & Şen, M. Enhanced bacterial rheotaxis in shear-thinning fluids. Proceedings of the National Academy of Sciences, 2024, 121(8): e2313594121.

[4] Dai, C., & Wang, Y. Thermo-bioconvection stability in gyrotactic microorganisms suspension saturated porous media with power-law fluid. Applied Mathematics and Mechanics, 2019, 40(11): 1617–1634.

[5] Moatimid, G. M., Hassan, M. A., & Mohamed, M. A. A. Pulsatile flow of Williamson nanofluid through porous medium with motile microorganisms. Journal of Porous Media, 2023, 26(4): 1–22.

[6] Theers, M., Westphal, E., Gompper, G., & Winkler, R. G. Modeling a spheroidal microswimmer and cooperative swimming in a narrow slit. Soft Matter, 2016, 12(47): 1–14.

[7] Theers, M., Westphal, E., Qi, K., Winkler, R. G., & Gompper, G. Clustering of microswimmers: interplay of shape and hydrodynamics. Soft Matter, 2018, 14(43): 8590-8603.

[8] Kai Qi, Hemalatha Annepu, Gerhard Gompper, et al. Rheotaxis of spheroidal squirmers in microchannel flow: Interplay of shape, hydrodynamics, active stress, and thermal fluctuations. Physical Review Research, 2020, 2(3): 1-14.

[9] Alan Cheng Hou Tsang, Pun Wai Tong, Shreyes Nallan, et al. Self-learning how to swim at low Reynolds number. Physical Review Fluids, 2020, 5(7): 1-9.

[10] Meng, F., Bennett, R. R., Uchida, N., & Golestanian, R. Conditions for metachronal coordination in arrays of model cilia. Proceedings of the National Academy of Sciences, 2021, 118(32): e2102828118.

[11] Steinkühler, J., Abrahamson, C. H., Agudo-Canalejo, J., Golestanian, R., Tullman-Ercek, D., & Kamat, N. P. Enzymatically-active bacterial microcompartments follow substrate gradients and are protected from aggregation in a cell-free system. bioRxiv, 2022.

[12] Hosaka, Y., Golestanian, R., & Daddi-Moussa-Ider, A. Hydrodynamics of an odd active surfer in a chiral fluid. New Journal of Physics, 2023, 25(8): 083046.

[13] Daddi-Moussa-Ider, A., Golestanian, R., & Vilfan, A. Minimum entropy production by microswimmers with internal dissipation. Nature Communications, 2023, 14(1): 6060.

[14] Yuto Hosaka, Michalis Chatzittofi, Ramin Golestanian, et al. Chirotactic response of microswimmers in fluids with odd viscosity. Physical Review Research, 2024, 6(3): 1-6.

[15] Piro, L., Vilfan, A., Golestanian, R., & Mahault, B. Energetic cost of microswimmer navigation: The role of body shape. Physical Review Research, 2024, 6(1): 013274.

[16] Tang, R., et al. Dynamic fluid layer around immotile yeast colonies mediates the spread of bacteria. Biophysical Journal, 2025.

[17] Liu, H., et al. Flagellum-driven motility enhances Pseudomonas aeruginosa biofilm formation by altering cell orientation. Applied and Environmental Microbiology, 2025.

[18] Kamdar, S., Shin, J., Leishangthem, P., & Bae, A. J. Colloidal solids enable enhanced motility in flagellated bacteria. Nature, 2022, 607(7918): 287–292.

[19] Wu, S., & Han, D. Dual-targeted nanovesicles eradicate intratumoral bacteria to potentiate immunotherapy in triple-negative breast cancer. Advanced Functional Materials, 2025.

[20] Chen, L., et al. Near-infrared-driven metal–organic frameworks-based nanorobots for controlled photothermal-chemical synergistic induction of cancer cell death. Advanced Robotics Research, 2025.

[21] Wu, Qianyuan; Yang, Cheng; et al. Hydrodynamic tearing of bacteria on nanotips for sustainable water disinfection. Nature Communications, 2023, 14:7794.

[22] Nganguia, H., & Palaniappan, D. Ciliary propulsion through non-uniform flows. Journal of Fluid Mechanics, 2024, 986: A14.

[23] Beris, A. N., et al. Recent advances in blood rheology: A review. Soft Matter, 2021, 17(23): 4766–4774.